

# Detection of Leak from Left Atrial Appendage Occlusion using Dielectric Imaging

Andy Adler, Mazen Albaghdadi, Usman Siddiqui, Keren Bitton-Worms, Noam Racheli, Urit Gordon and Karl-Heinz Kuck

**Abstract—Background:** Peri-device leak (PDL) following left atrial appendage occlusion (LAAO) may lead to an increased risk of thrombosis. However, current modalities for PDL detection, such as trans-esophageal echo (TEE) and cardiac CT do not provide quantitative measures of PDL.

**Objective:** to use dielectric imaging (DI) to measure PDL from a Watchman (WM) LAAO device.

**Methods:** A conductivity contrast agent is injected into the left atrium (LA) through the WM delivery system, while making DI measurements. Recordings are analyzed with a two-compartment model and the flow from the left atrial appendage (LAA) characterized by a “% clearance / beat” (CPB) parameter. With ethics approval, four dogs (26±1.8 kg) were anesthetized and ventilated. Body-surface electrodes were placed and impedance data continuously acquired. WM devices (0–35% oversized) were introduced and placed into the LAA. During the study, the WM was either fully or partial deployed. At each deployment level, 10 mL of conductivity contrast was injected through the WM delivery sheath. At twenty-two deployment conditions, Doppler-flow TEE measurements were made, and compared to the DI-based value.

**Results:** In all cases, CPB values correctly predicted the TEE-based assessment of PDL (100% sensitivity/specificity). The TEE leak size also corresponded to CPB values with a correlation of  $r=0.914$  ( $p<0.001$ ).

**Conclusion:** Using DI signals, the leak flow from the WM LAAO can be measured and yields comparative results to TEE for detection of PDL. The DI method requires no other imaging modality or ionizing radiation and iodine contrast agent injection.

## I. INTRODUCTION

For patients with nonvalvular atrial fibrillation (NVAf), the most common and serious risk is of thrombus formation and the resulting embolism leading to ischemic stroke. A risk of 1.5–3% per year has been identified in elderly patients and those with diabetes or hypertension, with the risk increasing to 6–10% in those with a higher CHA<sub>2</sub>DS<sub>2</sub>-VASc scores [16]. Medical treatment uses blood thinners (anticoagulation), which reduces stroke risk by 60% but increases the risk of serious bleeding complications by 0.2–0.5%. Anticoagulant therapy is contraindicated in many cases, and approximately 30% of NVAf patients do not receive it.

The most common site for thrombus formation is the left atrial appendage (LAA) [5]. Several medical devices have been developed to occlude the appendage and are referred to as Left

Atrial Appendage Occlusion (LAAO) devices. A successful occlusion mechanically prevents blood from entering the LAA and thus its potential to create thrombi which can subsequently embolize. LAAO devices are seeing increasing use in NVAf patients who cannot tolerate long-term anticoagulation [13]. Currently, the most commonly implanted devices are the Watchman (WM) (Boston Scientific, Marlborough, MA, USA) and the Amplatzer Amulet (Abbott point of care, Princeton, NJ, USA).

This study focuses on the Watchman (WM), although we are also investigating other devices. The main component of the WM is a nitinol mesh which is designed to seal the entrance of the LAA. This device is introduced intravenously through an introducer mechanism (see fig 1) and the compressed mesh is allowed to expand into the LAA. When correctly placed, the WM mesh and membrane act as a scaffold for tissue growth which completely seals the LAA. Data from trials of the WM suggest a reduction in hemorrhagic stroke but increased ischemic stroke compared to anticoagulants [10].

Incomplete closure of the LAA can result from incorrect sizing or placement of the WM device, and can result in leak around the periphery of the WM, referred to as “peri-device leak” (PDL). PDL is understood to indicate poor device placement and be associated with an increased risk of thrombotic events [15], [9], which may explain increases in ischemic stroke.

The current gold standard for detection of PDL is trans-esophageal echo (TEE), which uses a Doppler-ultrasound catheter placed into the esophagus and positioned to image the LAA and left atrium. For this application, Doppler TEE is used to measure the width of the flow in the peri-device area. The definition of “significant PDL” introduced during the WM trials is a residual flow in a  $\geq 5$  mm diameter gap between the device edge and the LAA tissue. According to [14], PDL occurs in 31% of patients but the rate varies according to the LAAO device. Unfortunately, the use of TEE has several operational disadvantages: it requires anesthesia for the patient, and thus a more complex and longer procedure with extra staff; it has a steep learning curve, is operator-dependent, and flow assessment is semi-quantitative. Additionally, factors such as acoustic shadowing and reverberation artefacts impede the acquisition of high-quality LAA images in many cases. We therefore identify a need for improved techniques to identify and qualify PDL [3].

In this paper, we describe the development, theory and pilot validation of a novel technology to detect and measure PDL. The basic concept is to introduce a conductivity-contrasting agent into the LAA, and to monitor the rate of dilution of

[In press: *IEEE Trans. Biomedical Engineering*, 2020-09-11]

This work was funded by K2 Medical Ltd.

Authors affiliations are as follows: Adler: Carleton University, Ottawa, Canada; Albaghdadi: Massachusetts General Hospital, Boston, USA; Siddiqui: University of Central Florida, USA; Racheli and Gordon: K2 Medical, Caesarea, Israel; Kuck: Asklepios Klinik St Seorg, Hamburg, Germany

the contrast out of the LAA through any leak present in the LAAO seal. We monitor the contrast agent using bioimpedance (or dielectric imaging, DI) measurements between the LAAO device and a body-surface electrode. A fractional-flow parameter, CPB (Clearance per Beat), is calculated which is analogous to an ejection fraction from the LAA. Our KALPA™ system also helps navigation, using additional electrodes to make low-frequency electrical stimulations on body-surface electrodes (at slightly different frequencies in each of the axes). The demodulated voltage,  $v$  for each axis gives a position estimate for each catheter electrode. Next, an inverse problem “V2R” is solved using the known catheter geometry to calculate the catheter position  $\vec{r}$  at each time point. This navigation technology has been described in [6], and is not further discussed in this paper.

Our approach offers numerous advantages. First, no new devices are required inside the patient; electrical measurements are made by connecting to the LAAO delivery cable, and the contrast agent is introduced through the device’s delivery sheath. The technique calculates a fractional-flow parameter, which can be easily related to the physiology of PDL. The use of a conductivity-contrasting agent allows several benefits. If a radiographic contrast agent for fluoroscopy is used, it also serves for DI measurements. If not using radiographic contrasts, conductivity contrasts can be hypertonic saline, saline or dextrose solutions, and are thus extremely safe [11]. For example, 10 mL of 3% saline (as used here) corresponds to 118 mg of Sodium, which is much less than a daily recommended intake of 2,300 mg [17]. This approach is automatic and user independent, in comparison to TEE, which requires a skilled operator and a complex and relatively time-consuming procedure.

In the remainder of this paper we explain the design an operation of our KALPA™ system, model its sensitivity, and describe robust calculation of the clearance parameter. A pilot trial is described from which results are compared to gold-standard TEE measurements.

## II. DEVICE OPERATION

The measurement configuration is illustrated in fig 1, showing an outline of the left atrium (LA) and appendage (LAA). The WM catheter is introduced intravenously and crosses through the RA to the LA through a septal puncture. Once the catheter is navigated to the LAA opening, the WM device is extruded from the sheath. The WM itself is made of nitinol, an alloy with shape memory, which assumes its designed shape after extrusion from the sheath and then fills the LAA opening, occluding it. A membrane attached to the metallic frame of the WM is initially somewhat porous, but later clots with blood, and acts as a scaffold for tissue growth. For verification of the placement of the WM, radio-opaque contrast agent is injected through the WM delivery sheath.

Our measurement uses the conductivity-contrasting properties of a contrast agent to analyze the peri-device leak from the WM. As shown in fig 1, four dilution processes occur, each with a corresponding rate. First, contrast is introduced ( $k_a$ ), some of which distributes into the LAA (rate  $k_{12}$ ) and

some of which leaves the LA through normal blood flow to the ventricle. The contrast agent which arrives in the LAA is distributed back to the LA (rate  $k_{21}$ ) and from the LA is eliminated at rate  $k_e$ . The key rate of interest is  $k_{21}$  which characterizes the leak rate. Here the leak is composed of both the PDL and the flow through the WM membrane, and we assume that the membrane flow is a smaller than the leak.

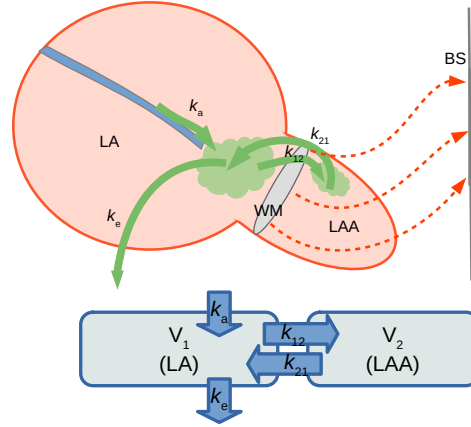


Fig. 1. Top: Schematic diagram of the WM passing through the left atrium(LA) and insertion into the left atrial appendage (LAA) opening. Red lines indicate current pathways from WM to a body-surface (BS) electrode. Green regions indicate contrast. Bottom: The equivalent two-compartment model. Rates,  $k$ ., correspond to processes: Contrast is introduced ( $k_a$ ), then distributes to LAA ( $k_{12}$ ), distributes back to LA ( $k_{21}$ ) and is eliminated from the LA ( $k_e$ ).

### A. Two-compartment models of flow from LAA

To determine the flow from the LAA, a two-compartment analysis is performed and the rate constant,  $k_{21}$ , estimated. Physiological compartment models are well understood [8]. The main result is that processes may be divided into “distribution” and “elimination” phases, as illustrated in fig 2, along with an example of recorded data with the filtering and exponential curve fitting, and its correspondence to the phases. When flow from the LAA is much smaller than that from the LA, and thus,  $k_{21} \ll k_e$ , the exponential rate during the elimination phase from the LAA,  $k_{elim,LAA} \approx k_{21}$ .

In order to noninvasively measure the concentration of contrast agent, we make electrical impedance (or dielectric imaging, DI) measurements from the metallic guidewire connected to the metallic WM device through to body-surface electrodes. This configuration is sensitive conductivity changes, primarily in the volume of the LAA, but also to a larger region near the WM mesh. Conductivity contrasts can be introduced which are either more conductive (e.g. hypertonic saline) or less conductive (e.g. radio-contrast agent) than blood.

In the next section, we describe the calculation of a parameter to characterize leak. Modelling of the accuracy and robustness of this system is given in section III.

### B. Data analysis algorithm

In operation, this system is designed to be used after placement of the WM into the LAA, and while it is still

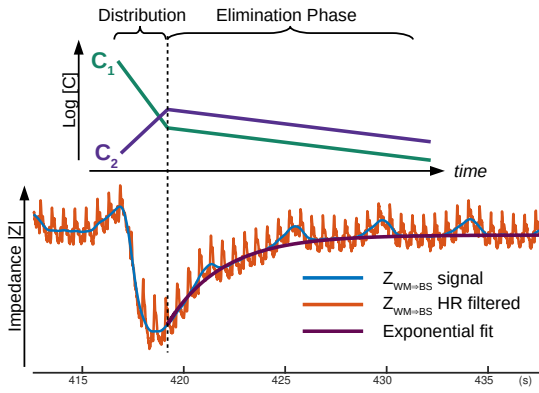


Fig. 2. Top: illustration of concentrations during the distribution and elimination phases. Bottom: Example measurements and the correspondence to the above phases. Contrast-agent injection started at  $t \approx 417$  s, The distribution-phase lasts about 0.3–0.5 s after which time the signals follow the elimination-phase rate.

attached to the guidewire. The WM is electrically connected via the guidewire to our system which measures the electrical impedance between electrodes at frequencies of 10–30 kHz. We analyze the absolute value,  $|Z_{WM \rightarrow BS}|$  of the impedance between the WM and a body-surface electrode. A contrast agent is injected through the WM sheath at a high rate, and some of the contrast passes through the WM membrane into the LAA. The contrast remaining in the LA rapidly leaves with the blood flow (rate  $k_e$ ). Subsequently, contrast agent leaves the LAA and the measured impedance changes, as shown in fig 2. The curve is fit to an exponential using the algorithm below, and time constant,  $\tau = k_{elim,LAA}^{-1}$  (units s) calculated. We then calculate a “clearance per beat” (CPB) parameter as:

$$CPB = \% \text{ cleared/beat} = 100 (1 - e^{-\lambda}) \quad (1)$$

where  $\lambda = (\tau \times HR)^{-1}$  and HR is the heart rate (in beats/s) calculated from a body-surface ECG signal. The CPB can be understood as the ejection fraction of the LAA, calculating the fraction of appendage volume exchanged each heart cycle. CPB characterizes the fractional peri-device leak; a decreased flow from the LAA leads to a decrease in  $k_{elim,LAA}$  and also in CPB.

The key challenge in calculating  $k_{21}$  is rejecting large unwanted signal contributions at the cardiac and breathing frequencies. We developed an algorithm to estimate and remove these interferences, which is illustrated in fig 3. The fitting algorithm goes through the following steps, starting with the absolute value of the measured impedance. Parameter searches for curve fits are implemented with a bounded nonlinear least-squares minimization, implemented using the “lmfit” python module. In all cases, multiple starting estimates are given to avoid local minima. For each algorithm analysis, data are processed from at least 10s before the event until the exponential has returned close to the baseline value. The key step in the algorithm is the removal of breathing-related interference, which is implemented by modelling and then subtracting the breathing-frequency signal.

#### 1. Signal normalization :

From the measured impedance,  $z_0 = Z_{WM \rightarrow BS}$ , The

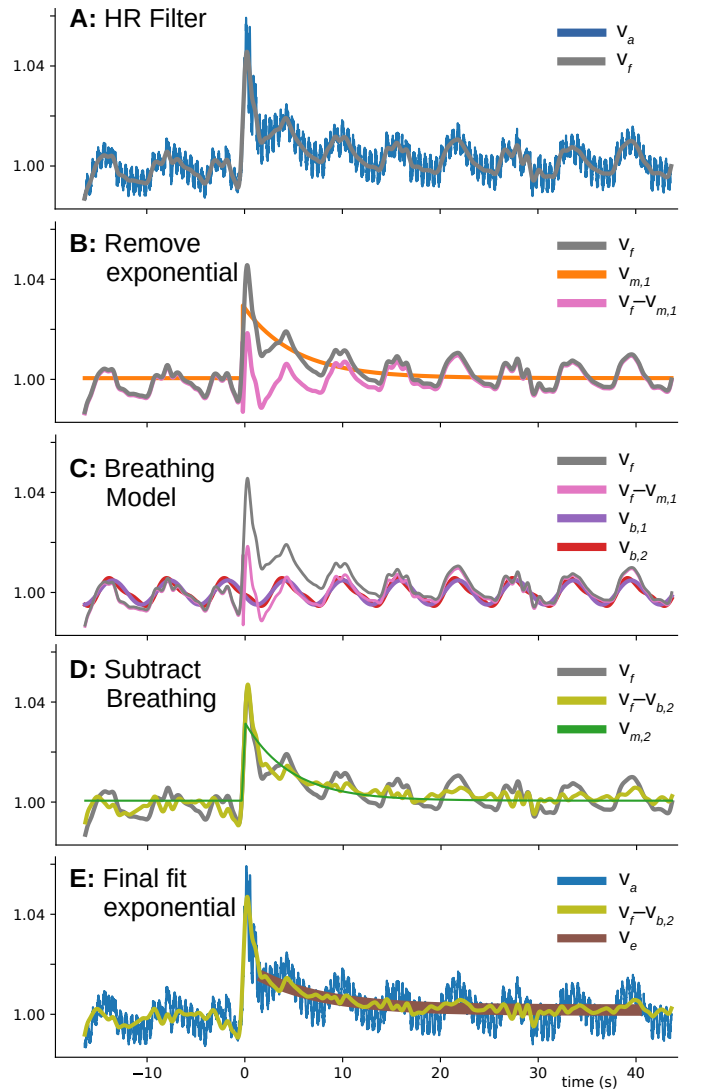


Fig. 3. Algorithm for robust curve fitting showing each stage of the processed signals. Algorithm details are in Sec II-B.

absolute-value of  $z_0$  is taken and normalized to a baseline  $z_{bl}$  set to the mean of the low-pass filtered last 5 s of the signal. A signal  $v_a = |z_0|/z_{bl}$  is calculated. This normalization means the true baseline value is close to one, and subsequent curve fitting can be within a restricted range.

#### 2. Heart-rate filtering (3 A):

The signal,  $v_a$ , is filtered at a frequency 20% below the estimated HR using a 4<sup>th</sup> order Butterworth filter, applied in the forward and reverse directions to ensure zero-phase offset. Edge effects are reduced using a padding with 15 s of the signal mean. A signal  $v_f$  is calculated.

#### 3. Breathing model estimation: A model of the shape of the breathing signal is created in steps (B & C).

##### 3a. Remove 1<sup>st</sup> pass exponential estimate (3 B):

An exponential model (2) based on five parameters ( $a, b, c, d, e$ ) is fit to  $v_f$ , where  $t_e = t - e$  is the time

offset to match the start of the exponential, and

$$v = \begin{cases} ae^{-t_e/b} + c & \text{if } t_e \geq 0 \\ a(1 - t_e/d) + c & \text{if } d < t_e < 0 \\ c & \text{if } t_e < d \end{cases} \quad (2)$$

From multiple fitting start points, the best fit (lowest residual),  $v_{m1}$  is subtracted from the signal to obtain  $v_{f1} = v_f - v_{m1}$ .

### 3b. Breath model (3C):

A breathing model is created from  $v_{f1}$  in two stages. First, a best-fit sinusoid,  $v_{b1}$  is fit to the signal, with parameters of amplitude, frequency and phase, from multiple starting points. Next, using the best-fit frequency and phase, three sinusoidal harmonics of the identified frequency are fit to the signal, to obtain the breath model,  $v_{b2}$ .

### 4. Removal of breathing (3D):

The breath model is removed from the filtered signal to obtain  $v_{f2} = v_f - v_{b2}$ . Next, in order to obtain an accurate estimate of the starting time of the exponential, exponential model (2) is fit to  $v_{f2}$  and the starting point parameter  $e$  retained.

### 5. Final exponential fit (3E):

A final exponential fit is obtained from the  $v_{f2}$  over an interval starting  $t_\Delta = 1.5$ s after the exponential peak (in order to ensure that we analyze only the elimination phase)

$$v = ae^{-t_e/\tau} + c \text{ for } t_e \geq t_\Delta \quad (3)$$

Finally, CPB is calculated (1) using the estimate  $\tau$  (and HR calculated from ECG data).

## III. SENSITIVITY MODEL

In this section, we build a simulation model of the measurements we perform in order to evaluate the range over which our estimates are appropriate. Our system uses two-compartment modelling of the concentration of contrast agent, but instead of directly measuring concentration, we measure the electrical impedance between the WM and a body-surface electrode. This potentially creates two uncertainties in the measurement. First, the sensitive region does not include only the LAA, but extends to other regions. This means that the measured signal is proportional to both concentrations  $C_1$  and  $C_2$ . Also, the measured impedance may not be necessarily proportional to the concentration of contrast. In this section we model these uncertainties.

Analysis is performed using a finite element model (FEM) illustrated in fig 4. This model includes seven body-surface electrodes in an otherwise-homogeneous elliptical thorax. It model part of the heart containing a spherical LA and spherical LAA, each with a thin myocardium region. The LA and LAA were connected at a cylindrical region specified to be the WM electrode. All electrodes used the complete electrode model [4], with a contact impedance per area,  $z_c = 0.01 \Omega/\text{m}^2$ . The WM was simulated to be a cylinder of diameter 3 cm and width 1 cm, leading to a contact impedance of  $10.6 \Omega$ , which is appropriate given the relatively low conductivity of nitinol metal. This FEM was created and solved using the EIDORS

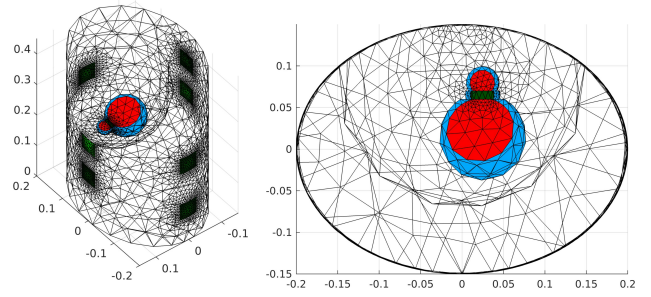


Fig. 4. FEM for calculation of sensitive regions in the model (red: regions with conductivity of blood, blue: regions with conductivity of tissue). A region is cut to visualize internal compartments. Left: side view, Right: view from above.

toolkit [2]. To accurately represent internal voltages, a fine mesh ( $\approx 245$  k nodes and 1.35 m elements) was used; however, for clarity of the illustration, fig 4 shows a lower resolution, at 19.7k elements. Tissue conductivities were specified as 0.7 S/m for blood, 0.2 S/m for myocardium and 0.4 S/m for other (background) tissue, based on [12].

First, the potential distribution was solved for current stimulation from the WM electrode to each of the body surface electrodes. Fig 5 shows the potential distribution in a transverse slice using an anterior ground electrode. The highest voltage gradients were in the immediate vicinity of the WM electrode and dissipated within a few cm of the WM itself.

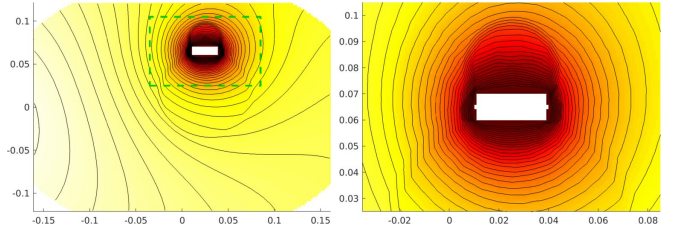


Fig. 5. Voltage distribution and equipotential lines in a transverse slices through the center of the WM in the FEM (Fig 4) of stimulation current flow between the WM electrode and a ground on the anterior body surface. Left: shows an inset (green box) into right around WM electrode A color mapping from white (zero) to red (maximum value) is used.

The sensitivity of the WM measurement is calculated for each element  $i$  in the FEM, as [1]:

$$S_i = \frac{1}{V_i} J_i(\sigma_b) = \frac{1}{V_i} \left. \frac{\partial F(\sigma)}{\partial \sigma_i} \right|_{\sigma_b} \quad (4)$$

where  $S_i$  is the sensitivity,  $V_i$  is the element volume, and  $J_i$  is the Jacobian calculated at a model conductivity  $\sigma_b$ . Here  $J_i$  is calculated as a perturbation  $\partial \sigma_i$  in element  $\sigma_i$  from the FEM,  $F(\sigma_b)$ . The sensitivity can be volumetrically displayed as the expected change in the measured value for a small increase in conductivity in each voxel. Fig 6 shows the sensitivity in the same transverse slice as voltages including iso-sensitivity surfaces.

Based on this analysis, we seek to determine what fraction of the sensitivity is concentrated in the LAA ( $S_{LAA}$ ) versus the LA ( $S_{LA}$ ). For this FEM geometry, the ratio between  $S_{LAA}/S_{LA} = 0.035$ . Over the volume of the LAA, there is

some variability in sensitivity, but the sensitivity is quite uniform; with a coefficient of variation,  $\sigma_S/\bar{S} = 0.47$ .

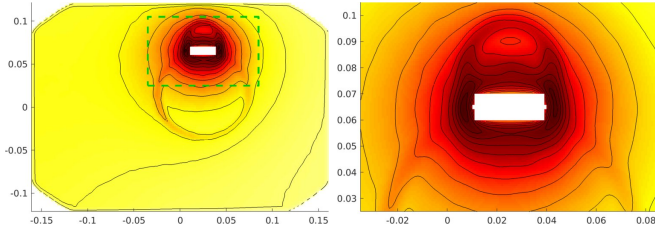


Fig. 6. Sensitivity and iso-sensitivity lines in a transverse slices through the center of the WM in the FEM (Fig 4) of stimulation current flow between the WM electrode and a ground on the anterior body surface. Left shows an inset (green box) into right around WM electrode. A color mapping from white (zero) to red (maximum value) is used.

#### A. Linearity of $\Delta Z$ with contrast

With this system, contrast agents can be selected to be either more or less conductive than blood ( $\sigma_b = 0.7 \text{ S/m}$ ) [12]. Defining  $\Delta\sigma = \sigma_c - \sigma_b$ , (with contrast agent conductivity  $\sigma_c$ ), we use 3% hypertonic saline, with  $\Delta\sigma = 4.50 - 0.70 = 3.8 \text{ S/m}$ , and iodine solution, with  $\Delta\sigma = 0.12 - 0.70 = -0.58 \text{ S/m}$ .

At low ionic concentrations, the conductivity of a sample varies linearly with concentration [7]. Thus, as the injected contrast agent dilutes into the blood, we expect the product of (contrast agent volume) $\times(\Delta\sigma)$  to remain constant. To describe the measured signals from this process, we simulate a spherical volume of 1 mL of undiluted contrast agent in the center of the LAA. At each step of the simulation this spherical volume is increased and the  $\Delta\sigma$  proportionally decreased until the volume covers the LAA. Contrast agents of 0.1 to 10 $\times$  the blood conductivity were simulated, and results are shown in fig 7, illustrating that sensitivity is close to linear over the dilution process.

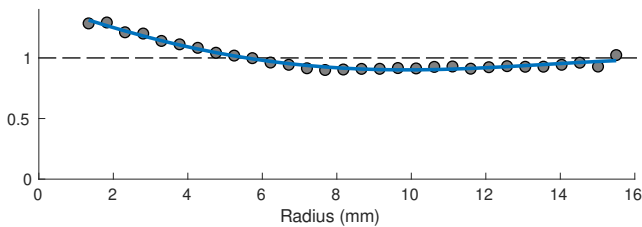


Fig. 7. Normalized sensitivity of a volume of contrast diluted into a sphere of blood, as a function of the radius dilution volume.

#### IV. EXPERIMENTAL METHODS

Pilot tests were conducted in an animal model to determine whether results were stable and the correspondence to gold standard measures. The study was reviewed and approved by the Animal Care and Use Committee (Ethics Committee number 37) of the Test Facility (Ethics approval K2 19-75 included in the project RYTHMOLOGIE 02-17). The animal research center (IMMR, Paris, France) received an agreement (n°75-14-01, 2014-08-18) for a period of 6 years by the “Direction Départementale de la Protection des Populations” of the French Authorities.

After premedication, a combination of Glycopyrrolate (0.01 mg/kg), Morphine (0.2 mg/kg) and Acepromazine (0.05 mg/kg) intramuscularly to sedate the animal, anesthesia was induced with an IV injection of Sodium Thiopental (5–10 mg/kg) and maintained by orotracheal intubation: Oxygen (100%) and Isoflurane (1–3%). Cefazolin (20 mg/kg) was administered intravenously (IV) to each study animal prior to the vessel access and every two hours thereafter for the duration of the intervention. ECG, blood pressure, end-tidal  $\text{CO}_2$  and core body temperature were monitored during the implantation procedure. Femoral access was obtained via intravascular sheath. A trans-septal puncture was done under an intra cardiac echo (ICE) and KALPA™ system guidance. The trans-septal sheath then exchanged with the device delivery sheath (14F WATCHMAN double curve) and flushed with heparinized saline (20 ml/h). WM devices were placed in the left atrial appendage under navigation of KALPA™ system and via trans-septal approach. Left atrial appendage (LAA) dimension were determined with the KALPA™ system and fluoroscopic with a 5F standard pigtail catheter and trans-esophageal echocardiography (TEE) measurements (0°, 45°, 90°, and 135°). The position of the device was verified by contrast agent injection via the delivery system and by TEE with the use of color Doppler ultrasound.

Two different contrast solutions were used: 3% hypertonic saline (producing an increase in conductivity) and iohexol (Omnipaque, GE Healthcare) radiographic contrast agent (producing a decrease in conductivity). Contrasts were introduced via a rapid bolus injection through the WM sheath while the guidewire was still connected to the WM (and thus 2–5 mm away). Contrast would thus pass through the WM membrane and into the LAA. In each animal, the WM was adjusted to achieve different levels of seal and thus to vary the PDL. At each WM adjustment level, several contrast agent injections and measurements were made, using both the contrast types.

#### V. RESULTS

In the pilot test, four female dogs 23–27 kg were implanted with the WM LAAO device (18–20 mm, Watchman FLX next-generation device (Boston Scientific, Marlborough, MA, USA) under fluoroscopic and KALPA™ system guidance.

Data were collected for 109 seal-test events, including 82 using saline and 27 using iodine contrast agents. For each event, impedance data were analyzed using the presented algorithm. Fig 8 shows examples of raw  $|z|$  data and the implemented curve fitting, while fig 9 shows example Doppler TEE images.

Of the seal-test events, 18 were conducted at the same time as TEE measurements. The presence of PDL was defined as a TEE measurement of the leak width above 1 mm (corresponding to the definitions of the [9]). Using this definition, these cases were separated into “PDL” and “no PDL” categories. Fig 10 (Left) shows the CPB (% clearance/beat) and the corresponding TEE values. By setting a threshold CPB value between 5 and 7%/beat, it was possible to correctly classify all tests (i.e. 100% sensitivity and specificity). The correlation between CPB and TEE values was  $r=0.914$ .

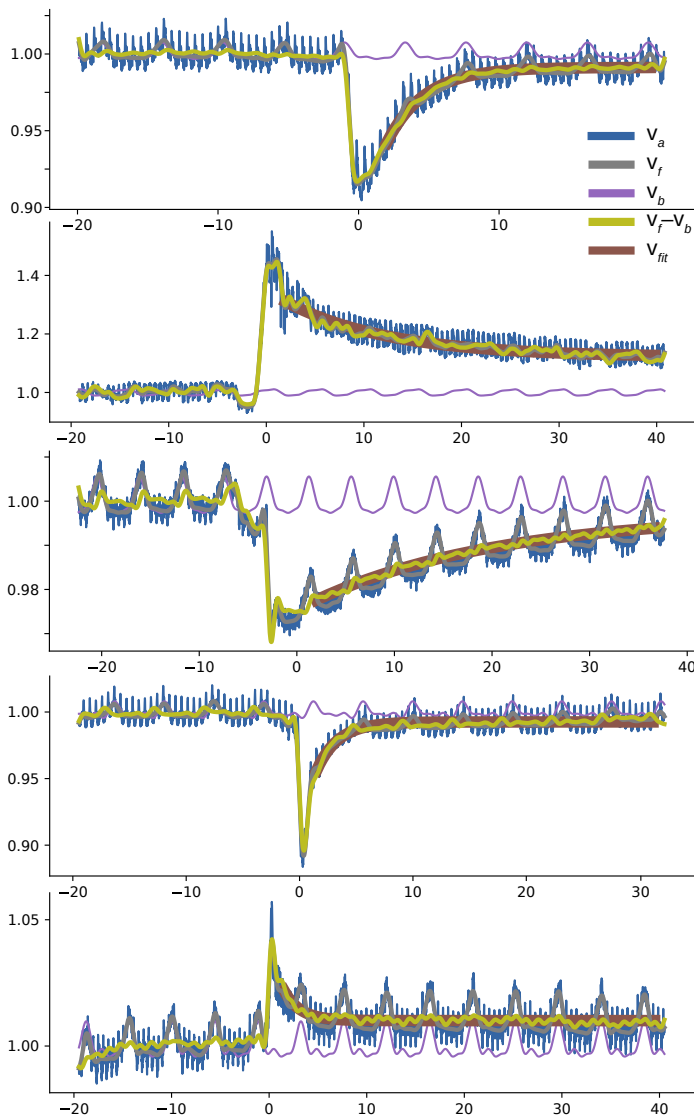


Fig. 8. Sample results showing the measured impedance data and the curve fitting parameters calculated by the algorithm. Curves with increasing impedance are due to iodine contrast, while those with decreasing impedance are due to saline contrast.

Using these values, we tested the null hypothesis that CPB does not vary between “PDL” and “no PDL” cases. Because of the relatively small number of measurements, and as normality cannot be assumed, we used the nonparametric Mann-Whitney “U” test. Using a two-sided test,  $p = 0.00065$ ; we thus reject  $H_0$ , and conclude that CPB varies significantly in the presence and absence of PDL.

## VI. DISCUSSION

In this paper, we are motivated by the problem of identifying peri-device leak in left-atrial appendage occlusion device placements. We describe a novel approach to measure it using injection of a conductivity-contrasting agent into the LAA, and measurement of dielectric impedance between the metallic mesh of the LAAO device and a body-surface electrode. The rate of leak from the device is characterized by a parameter “clearance per beat” (CPB). The device was then evaluated

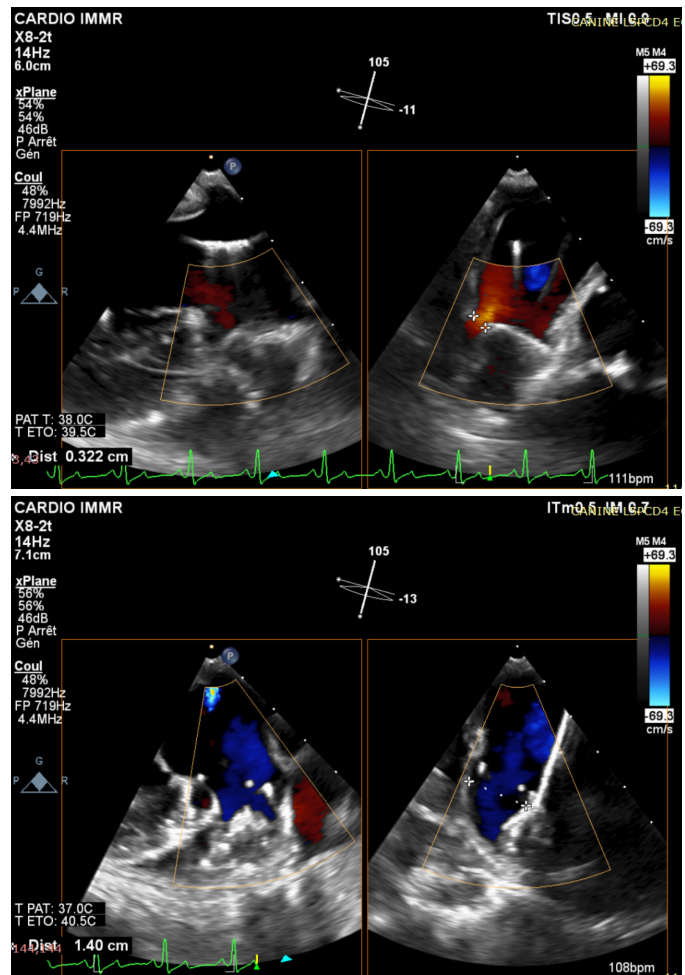


Fig. 9. Sample Doppler TEE images illustrating the calculation of the leak distance. The “+” cursors are placed on the WM and adjacent LAA position and the distance calculated. Top: TEE=3.22 mm and CPB=12.3%, Bottom: TEE=14.0 mm and CPB=44.0%.

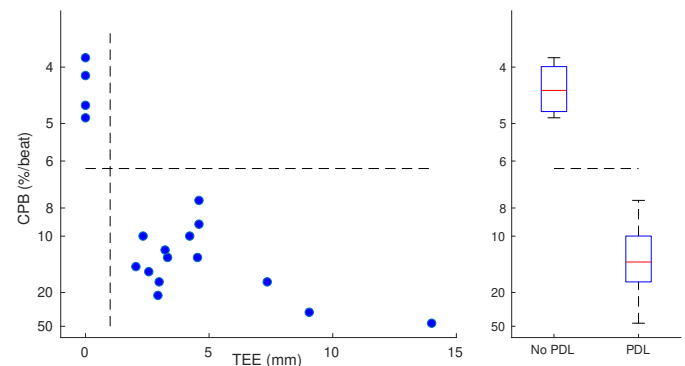


Fig. 10. Correspondence of CPB (%/beat) values (inverse scale) vs TEE (mm). (Left) scatterplot and (Right) boxplot according to the presence or not of peri-device leak.

in pilot experiments in animals against TEE measurements, where a 100% sensitivity/specificity was seen.

In the past decade, there has been an increasing appreciation of both the prevalence of atrial fibrillation and of its consequences, most seriously the risk of stroke from emboli. Since the LAA is the most common site for thrombus formation,

there is a clear need for medical devices to occlude the LAA, especially for patients who cannot tolerate long-term anticoagulation. The current gold-standard for validation of placement is TEE, which has numerous disadvantages, both technically, and in terms of the requirement for a more complex, longer procedure with additional trained staff.

The approach we describe here is designed to be simpler to implement and easy to interpret. No new internal devices are required, since electrical connection are made to the device guidewire and body-surface electrodes. Contrast agents are completely safe (hypertonic saline or dextrose solution giving an increased or decreased conductivity) or can be made from radiographic contrast solutions. Data are automatically analyzed within seconds of injection, and a parameter calculated which can be related to the ejection fraction of the LAA. One novel possibility is to perform multiple PDL tests throughout the process of device placement to provide extra information.

Our work has several limitations. First, this is pilot study with a small number of animals. All animals were healthy, and thus potentially dissimilar to LAAO device patients. In each experimental animal, multiple measurement scenarios were created by changing the configuration of an individual WM device, potentially leading to correlations between measurements. We only used the WM flex device for this study, although the underlying technology is applicable to many LAAO devices. In terms of the analysis algorithm, we currently model breathing as Fourier components of a single frequency. This is suitable for ventilated, anesthetized patients; however, the breath-modeling algorithm will need to be modified for spontaneously-breathing patients. Additionally, the CPB parameter assumes a constant HR, which may not be valid, especially in patients with arrhythmia.

In addition to pilot tests in animals, we develop a numerical model to evaluate the sensitivity and linearity. Model results suggest that the system is sensitive primarily to the LAA and the region of the LA close to the WM mesh with lower sensitivity elsewhere (fig 6). Since the flow from the LA is much greater than from the LAA,  $k_e \gg k_{elim,LAA}$ , and the elimination phase is dominated by the LAA concentration after a few heart beats. We use  $t_\Delta = 1.5$  s to account for this delay. Additionally, the sensitivity is roughly uniform throughout the LAA region and as a function of dilution of the contrast, which means that the estimated parameter is less affected by the position or rate of dilution of the contrast agent into the blood. This approach does have some disadvantages with respect to fluoroscopy and TEE, in that it provides a single parameter and not an image. It is thus not possible to tell from which part of the LAAO device leak is occurring.

In summary, we describe a novel technique to measure peri-device leak from a LAAO device, and show pilot experimental results in which the technology accurately distinguishes leak from non-leak cases.

## VII. CONCLUSION

We describe a new technique to measure peri-device leak around a left-atrial appendage occlusion device, by injecting conductivity-contrasting fluid into the appendage and measuring the impedance between the device and a body surface

electrode. The fractional leak flow is calculated from a two-compartment model of the impedance signal. In a pilot experiment, the leak flow from a Watchman LAAO device could be measured and gave comparable results to the current gold standard for detection of PDL. Our impedance-based method requires no other imaging modality or ionizing radiation and iodine contrast agent injection.

## REFERENCES

- [1] A Adler, A Boyle, "Electrical Impedance Tomography: Tissue Properties to Image Measures" IEEE T Biomed Eng, 64:2494–2504, 2017.
- [2] A Adler, WRB Lionheart, "Uses and abuses of EIDORS: An extensible software base for EIT", Physiol Meas 27, S25–S42, 2006.
- [3] M Albaghdadi, et al "Peri-Device Leaks After Percutaneous Left Atrial Appendage Closure: Clinical Significance and Unmet Diagnostic Needs" In press: *Structural Heart*, August 2020.
- [4] K-S Cheng, et al "Electrode models for electric current computed tomography." IEEE T Biomed Eng, 36:918-924, 1989.
- [5] A Cresti, et al, "Prevalence of extra-appendage thrombosis in non-valvular atrial fibrillation and atrial flutter in patients undergoing cardioversion: a large transoesophageal echo study" EuroIntervention 15:e225-e230, 2019.
- [6] E Dichterman, et al "Systems and Methods for Reconstruction of Intra-body Electrical Readings to Anatomical Structure" WO/2018130974, 2018.
- [7] CW Davies, "Ion Association", Science, 143:37, 1962.
- [8] M Gibaldi, D Perrier, Pharmacokinetics, 2<sup>nd</sup> ed.; New-York: Marcel Dekker, 1982.
- [9] Gianni C, et al "Clinical Implications of Leaks Following Left Atrial Appendage Ligation With the LARIAT Device." JACC Cardiovascular interventions. 9:1051–1057, 2016.
- [10] DR Holmes Jr, et al "Prospective randomized evaluation of the Watchman Left Atrial Appendage Closure device in patients with atrial fibrillation versus long-term warfarin therapy: the PREVAIL trial." J Am College of Cardiology. 64:1–12, 2014.
- [11] S-J Huang, et al, "Efficacy and safety of hypertonic saline solutions in the treatment of severe head injury" Surgical Neurology, 65:539–546, 2006
- [12] IT'IS Foundation (2018) "Tissue Properties Database V4.0", DOI: 10.13099/VIP21000-04-0
- [13] CT January, et al, "Focused Update of the 2014 AHA/ACC/HRS Guideline for the Management of Patients With Atrial Fibrillation" J Am College of Cardiology. 74:104–132, 2019.
- [14] S Lindner, et al "Assessment of peri-device leaks after interventional left atrial appendage closure using standardized imaging by cardiac computed tomography angiography" Int J Cardiovascular Imaging, 4:725–731, 2019
- [15] A Nguyen, et al "Peridevice Leak After Left Atrial Appendage Closure: Incidence, Risk Factors, and Clinical Impact" Canadian Journal of Cardiology 35:405–412, 2019.
- [16] Stroke Risk in Atrial Fibrillation Working Group, "Independent predictors of stroke in patients with atrial fibrillation: a systematic review. Neurology" 69:546–54, 2007.
- [17] PK Whelton, et al "Sodium, Blood Pressure, and Cardiovascular Disease" Circulation, 126:2880–2889, 2012